

***Ab Initio* Raman Spectra of β -Lactamase Inhibitor Intermediates Bound to E166A SHV β -Lactamase**

Andrea Miani,[†] Marion Skalweit Helfand,[‡] and Simone Raugei*,[†]

SISSA and INFM-DEMOCRITOS center via Beirut 2, I-34014, Trieste, Italy, and Louis Stokes Cleveland Department of Veterans Affairs Medical Center, Cleveland, Ohio 44106

Received March 20, 2009

Abstract: The assignment and the analysis of the experimental vibrational Raman spectra of enzyme bound β -lactamase inhibitors may be of help to understand the mechanisms responsible for bacterial drug resistance. We present a computational study of the structural and vibrational properties of clavulanic acid and tazobactam intermediates, two important β -lactamase inhibitors, bound to the singly mutated E166A SHV β -lactamase in aqueous solution by hybrid molecular mechanics/quantum mechanics (QM/MM) simulations at ambient conditions. We compare the Raman spectra obtained from the time autocorrelation function of polarizability tensor as obtained from a QM/MM protocol to those obtained from the instantaneous normal modes analysis performed on top of the QM/MM trajectory in order to establish the accuracy of these two computational methods and to review the previously made assignments. It is shown that the O=C—C=C—NH— trans-enamine moiety symmetric and asymmetric stretchings are strongly coupled with the N—H in-plane rocking and originate the band structure between 1600 cm^{-1} and 1640 cm^{-1} . Results indicate also that to properly describe Raman scattering properties of the trans-enamine intermediate, it is crucial to include both mechanical (beyond the second derivative of the potential energy at equilibrium) and electrical (beyond the first derivative of polarizability) anharmonicity. In addition, we show that the environment electrostatic field dynamically modulates the Raman activity, enhancing or inhibiting it.

1. Introduction

Raman microscopy and spectroscopy have been extensively employed to study relevant problems of biological interest, such as the β -lactamase mediated bacterial resistance to antibiotics (refs 1–5 and references therein), a major clinical problem worldwide. Inhibitors are usually employed to enhance the therapeutic efficacy of specific antibiotics, but several aspects of the involved reactions are still to be understood.

Raman microscopy together with X-ray crystallography, in particular, establishes a correlation between the activity and the degree of stability of the trans-enamine intermediates formed during the inhibition reaction by clavulanic acid,

tazobactam (Figure 1a), and sulbactam, the only three inhibitors clinically available so far.⁶ The majority of studies looked at the inhibitor intermediates formed with E166A SHV, a mutated β -lactamase, which prevents the deacylation of the enzyme allowing trapping of the intermediates for X-ray crystallographic investigations (Figure 1b). A very recent Raman crystallographic study of the reaction intermediates from wildtype SHV has also been reported.⁵ Difference Raman spectra were obtained subtracting from the recorded spectrum of the inhibitor bound to the protein that of the protein alone.^{1,4,5} The assignment of the strong band observed in the difference Raman spectra at 1592, 1599, and 1605 cm^{-1} for tazobactam, sulbactam, and clavulanic acid, respectively, to the trans-enamine stretching mode was crucial to establishing such a correlation. The assignment was made on the grounds of *ab initio* calculations performed on simplified gas phase models and confirmed experimentally by the observed shift of the same peak in D_2O due to isotopic

* Corresponding author e-mail: raugei@sissa.it.

[†] SISSA and INFM-DEMOCRITOS center via Beirut 2.

[‡] Louis Stokes Cleveland, Department of Veterans Affairs Medical Center.

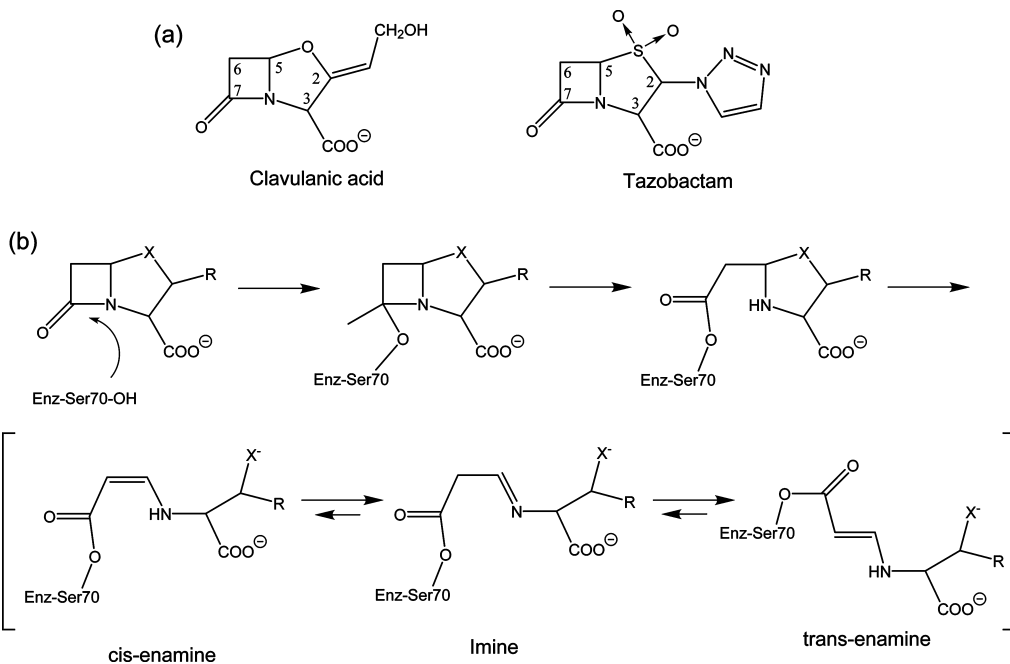


Figure 1. (a) Chemical structure of the two β -lactamase inhibitors considered in the present study (clavulanic acid and tazobactam). (b) Proposed reaction scheme for beta-lactam-based inhibitors with the deacylated deficient E166A SHV β -lactamases. Notice that, in the case of clavulanic acid, the reaction further proceeds with the intermediate decarboxylation.

substitution. The assignment of the observed isotopic shift, on the other hand, was again done following suggestions deriving from *ab initio* on the same model. Despite the number of investigations reported in the literature, the detailed understanding of the spectral features, especially in the region around 1600 cm^{-1} , has not been achieved yet (see for instance refs 1, 4, and 5). The purpose of this work is dual: (*i*) contribute to the assignment of the SHV β -lactamase/inhibitor Raman spectra and (*ii*) assess the accuracy achievable with the available quantum-chemistry methods for calculating vibrational spectra for complex systems of biological interest.

The calculation of vibrational spectra for solvated systems of biological interest is a very demanding task. Standard classical force fields are not sufficiently accurate to reproduce the experimental vibrational spectra. On the other hand, quantum mechanics (QM) simulations are still too computationally demanding. Even if QM methods could be employed for simulating the system, the calculation of the dielectric (polarizability) tensor for the whole system (or of a part of it) is problematic. For clavulanic acid in aqueous solution, we have recently shown⁷ that hybrid quantum mechanics/molecular mechanics (QM/MM) methods, in which the solute is treated quantum mechanically and the solvent with an empirical potential, are able to reproduce both the solute solvation and vibrational structures when compared to the more demanding full QM simulation, in which both the solute and the solvent are treated quantum mechanically. Moreover we have proposed a simplified and computationally efficient protocol to calculate the polarizability tensor for the whole system.⁷ In this work, we employ the same QM/MM simulations to calculate the Raman spectra of *h*- and *d*-clavulanic acid and *h*- and *d*-tazobactam trans-enamine intermediates bound to the E166A SHV β -lactamase, using the time autocorrelation functions (ACF) for-

mism. We then compare the QM/MM spectra to those obtained from the Instantaneous Normal Modes Analysis (INMA),^{8–10} probably the only other available method so far for calculating (routinely) vibrational spectra for such complex systems, in order better understand and compare the advantages and the limitations of techniques for the calculation of Raman spectra of complex systems.

The paper is organized as follows: in the next section (Section 2) the computational details of the methods employed in this work are explained. In Section 3, INMA and QM/MM results are discussed and compared to the available experimental data. Particular attention is dedicated to possible sources of error in the calculation of spectra, especially to statistical sampling errors. Finally, the main points of our study will be summarized in Section 4.

2. Computational Methods

2.1. Computational Models. The clavulanic acid and tazobactam intermediates bound to the deacylation-deficient E166A SHV β -lactamase (PDB structures 2A49 and 1RCJ, respectively) have been studied by long time scale classical molecular dynamics (MD) simulations based on the Amber¹¹ force field and TIP3P¹² water at atmospheric pressure and room temperature, followed by hybrid density functional theory (DFT)/molecular mechanics simulations.

The clavulanate and tazobactam-E166A SHV crystal structures include one and two nonstandard molecules, respectively: HEPES (4-(2-hydroxyethyl)-1-piperazin ethanesulfonic acid) used as buffer and Cymal 6 (cyclohexyl-hexyl-beta-D-maltoside, MA4 hereafter) used as nonionic detergent in the crystallization procedure. HEPES is present only in the 2A49 structure and is found adjacent to the intermediate, being the sulfonic group near the ester group of the trans-enamine (Figure 2). The 1RCJ structure does not contain

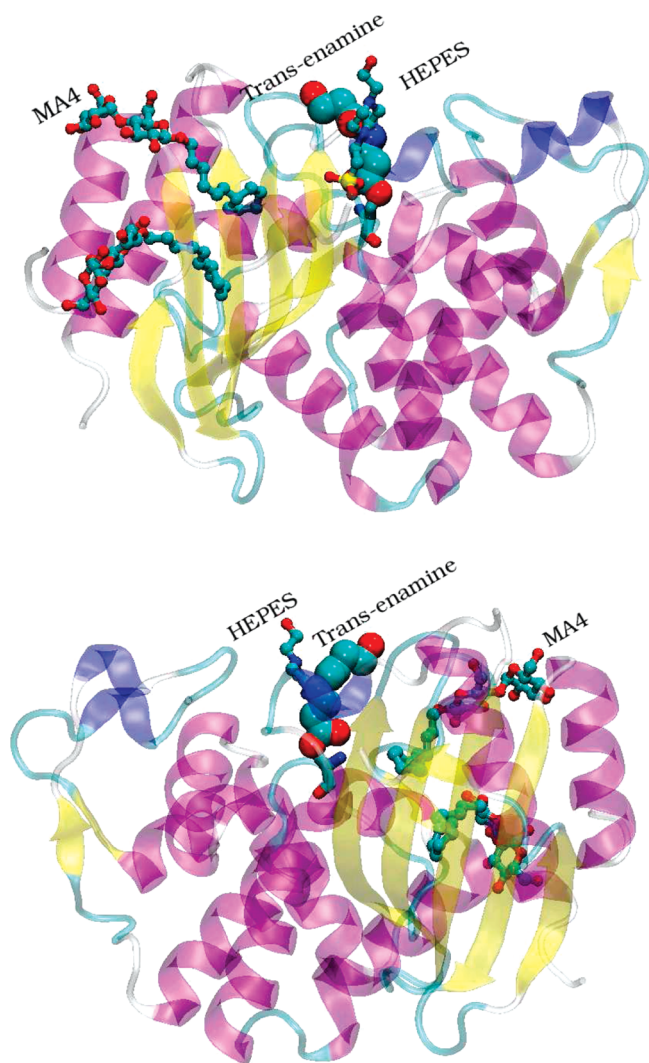


Figure 2. Two different views of the trans-enamine SHV β -lactamases intermediate crystallographic structure (PDB entry 2A49). The protein scaffold is shown in a cartoon representation, the trans-enamine moiety as spheres, the HEPES and the MA4 molecules in ball and sticks.

this molecule likely because of the bulky triazolyl moiety in tazobactam. In both crystal structures there are also two MA4 intercalated between helix 10 and helix 11 at more than 13 Å from the active site. Simulations were performed including these molecules. We remark that test simulations carried out without the MA4 molecules indicated that their insertion does not alter neither the protein structure or its flexibility. A further difference between the two crystal structures is the absence of the C3 carboxylate group in the intermediate from clavulanic acid (Figure 1).

The experimental Raman spectra were recorded during inhibitor soaking experiments for clavulanate and tazobactam¹ on a E166A SHV β -lactamase microcrystal. Simulations and the subsequent calculation of the Raman spectra were performed in an aqueous solution-like environment. This choice was dictated by the larger computational effort required to study the crystal phase as the crystal unit cell contains four protein molecules. On the other hand, although the catalytic pocket is at the protein surface, the trans-enamine intermediate is buried into the protein scaffold and

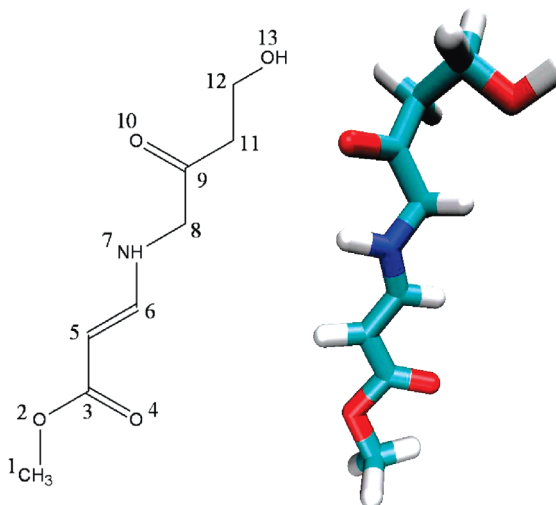


Figure 3. 2D and 3D structure of the quantum model used to describe the clavulanate trans-enamine intermediate together with the labeling of the heavy atoms employed in this work. The quantum region is terminated with the methyl group at position 1.

only the terminal part of the chain is exposed to water. In the crystal, the tail of the trans-enamine is separated from the nearest protein molecule by at least four water layers. Therefore, the major electrostatic influence to the static polarizability of the intermediate comes from the protein, the HEPES molecule (in the case of the intermediate from clavulanic acid), and the surrounding solvent. These facts make us confident that the spectrum calculated on a solution model of the protein adduct well represents the spectrum recorded on the microcrystal.

2.2. Classical Molecular Dynamics Simulations. The clavulanate and tazobactam intermediates as well as HEPES and MA4 were parametrized using the General Amber Force Field (GAFF),¹³ whereas the Restrained ElectroStatic Potential (RESP) charges were calculated at density functional theory level (B3LYP/6-31+G(d)¹⁴ using Antechamber¹⁵ and Gaussian.¹⁶ The proteins were immersed in an orthorhombic box containing 14082 and 13861 TIP3P¹² water molecules for clavulanate and tazobactam, respectively, plus sodium counterions to guarantee electroneutrality. The systems were first equilibrated for about 0.5 ns letting only water relax at room temperature. Then all the atoms were left free to move, and the temperature was gradually increased from 0 K to room temperature. The simulation was then continued at ambient conditions for 9 ns employing the Berendsen thermostat and barostat.¹⁷ The Amber package¹¹ was used to equilibrate the systems, whereas the Gromacs program was subsequently employed¹⁸ to run the production dynamics.

2.3. Hybrid QM/MM Molecular Dynamics Simulations. Starting from a snapshot of the classical MD simulations, a constant volume hybrid Quantum Mechanics–Car–Parrinello (CP)/Molecular Mechanics^{19–22} simulation was performed at room temperature partitioning the system into a quantum part, which includes the inhibitors and the Ser70 atoms up to the C_β (Figures 3 and 4), and a classical part, including water, buffer and detergent molecules, and the remaining part of the protein. The QM region was described within gradient-corrected DFT using the Becke²³

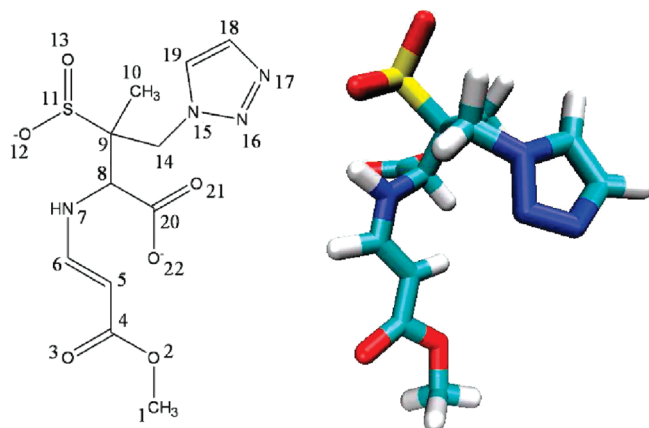


Figure 4. 2D and 3D structure of the quantum model used to describe the tazobactam trans-enamine intermediate together with the labeling of the heavy atoms employed in this work. The quantum region is terminated with the methyl group at position 1.

and Lee, Yang, and Parr²⁴ (BLYP) exchange and correlation energy functional. Norm-conserving Martins-Troullier pseudopotentials²⁵ were used to describe the interactions between the core and valence electrons for all atoms but for hydrogens, for which a von Barth-Car pseudopotential²⁶ was used to smooth out the short-range Coulombic nuclear potential. The Kohn–Sham orbitals of valence electrons were expanded in plane waves with kinetic energy up to 70 Ry. The electrostatic coupling between the QM and the MM region is calculated by using the full Hamiltonian scheme proposed by Rothlisberger and co-workers^{21,22} as implemented in the CP code CPMD 3.10.²⁷ Explicit electrostatic interactions between the quantum and the classical part were taken into account for residues and water molecules having at least one atom within 5.3 Å from any atom of the inhibitors. Electrostatic interactions between dynamically fitted D-RESP point charges²² located on the QM atoms and the force field RESP²⁸ charges on the MM atoms were considered for the remaining MM atoms within 10.6 Å from the QM part. Finally, electrostatic interactions between the MM atoms and a multipole expansion of the QM charge distribution were considered for MM atoms beyond 10.6 Å. The Car–Parrinello equations of motions were integrated using a fictitious electronic mass of 600 au and a time-step of 0.12 fs. The system was equilibrated for 1 ps with a Nosè–Hoover chain of thermostats,²⁹ and then the trajectory was sampled in the microcanonical ensemble for about 10 ps for the intermediate from tazobactam and about 24 ps for the intermediate from clavulanic acid taking advantage of its smaller size and therefore of its minor computational cost.

2.4. Raman Spectra. The vibrational Raman activity was calculated both via the standard quantum chemistry INMA method^{8–10} and the time ACF formalism with a QM/MM protocol previously established.⁷ In the latter, the time evolution of the polarizability tensor was calculated from the QM/MM trajectory extracting one configuration every 3.0 fs for clavulanate and 2.4 fs for tazobactam. These time intervals ensure the proper sampling of the mode with shortest vibrational period (that of N–H stretching vibration). The polarizability tensor for the chosen molecular configura-

tions was then evaluated using the BLYP density functional and the cc-pVDZ basis set,³⁰ including the effect of the surrounding electrostatic potential due to the solvent and protein.^{31,32} We included the charges of the whole protein and of a spherical shell of 25 Å of TIP3P water molecules around the inhibitors as obtained from the QM/MM trajectory. The same exclusion rules for the electrostatic interactions employed in the QM/MM simulation were used. It was previously noticed that, in the case of aqueous solutions, the polarizability tensor is not significantly affected when limiting the calculation to two shells of charges only.⁷ The calculation of the polarizability tensor for each snapshot required about 30 min for clavulanate, and 1 h and 25 min for tazobactam on one core of an AMD Opteron Dual Core (2.6 GHz) processor with the Gaussian03 package.¹⁶ To reduce the required computational time for tazobactam without significantly affecting the accuracy of the calculated polarizability, we employed the pseudopotential LanL2ZD for the sulfur atom.³³

As previously reported,⁷ the following expression for the Raman scattering cross section per unit of solid angle and unit of frequency, $I_{\perp}(\omega)$, observed perpendicularly to the incident light of frequency ω_0 can be written as^{34,35}

$$I_{\perp}(\omega) \propto (\omega_0 - \omega)^4 \int dt e^{-i\omega t} \langle \text{Tr} \beta(0) \cdot \beta(t) \rangle_{qm}^+ = (\omega_0 - \omega)^4 C_{qm}(\omega) \quad (1)$$

with β being a traceless anisotropic part of our systems polarizability, α , calculated in a molecular fixed frame, $\beta = \alpha - \bar{\alpha} \mathbf{I}$, where $\bar{\alpha}$ is the average of the polarizability tensor trace, and \mathbf{I} is the unit tensor. After diagonalizing the polarizability tensor, the Raman scattering activity can then be obtained by calculating the Fourier transform of its symmetrized quantum mechanical ACF, $C_{qm}(\omega)$, which, following Bader and Berne,³⁶ is approximated in terms of the corresponding classical ACF, $C_{cl}(t)$, as

$$C_{qm}(\omega) = \frac{\hbar\omega}{2k_B T} \coth\left(\frac{\hbar\omega}{2k_B T}\right) C_{cl}(\omega) \quad (2)$$

where \hbar is the reduced Planck constant.

The vibrational Raman spectra for our systems were also obtained using the INMA protocol.^{8–10} INMA vibrational modes are calculated for an instantaneous relaxed configuration in the confinement potential of the environment. For this reason, they are often referred to as “quasi-harmonic”. Thirty-two frames equispaced in time were selected from the QM/MM trajectories of *h*-, *d*-tazobactam and clavulanate and from the classical trajectory for *h*- and *d*-clavulanate. For each frame, the QM subsystem was then relaxed keeping the classical part of the system fixed at the given geometry and gradually annealing the quantum ions up to a residual force on each QM atom of 10^{-5} a.u. The harmonic frequencies and the derivatives of the polarizability tensor for the optimized structures were then obtained using Gaussian,¹⁶ including the external charges of the remaining system, for the vibrational analysis. The calculation was performed by using the cc-pVTZ basis set. The BLYP exchange and correlation functional was employed. In the case of the

intermediate from clavulanic acid, BLYP results were verified against the more accurate hybrid B3LYP exchange and correlation functional.¹⁴ Harmonic Raman activities were obtained from the expression

$$\tilde{I}_{\perp}(\omega_i) = 45\alpha'(\omega_i)^2 + 7\beta'(\omega_i)^2 \quad (3)$$

where \tilde{I}_{\perp} refers to the total Raman scattering activity determined by the perpendicular component of the incident light electric field with respect to the scattering direction. The terms α' and β' appearing in \tilde{I}_{\perp} are defined as

$$\alpha' = \frac{1}{3}(\alpha'_{x,x} + \alpha'_{y,y} + \alpha'_{z,z}) \quad (4)$$

and

$$\beta'^2 = \frac{1}{2}[(\alpha'_{x,x} - \alpha'_{y,y})^2 + (\alpha'_{x,x} - \alpha'_{z,z})^2 + (\alpha'_{y,y} - \alpha'_{z,z})^2 + 6(\alpha'_{x,y}^2 + \alpha'_{x,z}^2 + \alpha'_{y,z}^2)] \quad (5)$$

where the prime indicates the derivative of the polarizability tensor elements with respect to the i -th normal mode.^{37,38} To calculate the relative Raman cross sections for the harmonic modes in the Stokes spectral region, the Raman scattering activity has been corrected with the factor

$$I_{\perp}(\omega_i) \propto \frac{(\omega_0 - \omega_i)^4}{\omega_i[1 - \exp(-\hbar\omega_i/k_B T)]} \tilde{I}_{\perp}(\omega_i) \quad (6)$$

where $\hbar = h/2\pi$ is the reduced Planck constant, k_B is the Boltzmann constant, and T is the absolute temperature. INMA spectra were simulated assuming a Lorentzian band shape with a bandwidth of 15 cm^{-1} . We remark that in ref 7 the formula for the intensity in the anti-Stokes region was erroneously reported. However in the calculations the proper expression for the Stokes region was employed.

Raman spectra for deuterated intermediates were also obtained via both QM/MM simulations and INMA. The calculation with QM/MM dynamics requires additional simulations where an H atom is replaced by a D isotope. In contrast, standard normal-mode analysis allows one to quickly evaluate isotopic effects by simply modifying the mass-weighted Hessian matrix since, in the Born–Oppenheimer approximation, the Hessian does not depend on the isotopic composition. We performed calculations for two different isotopic H/D substitutions. The first one concerns the enamine N–H hydrogen, which most easily undergoes H/D exchange with the solvent.^{1,5} In addition, also the possibility of a double deuterium exchange is taken into account. Indeed, it has been recently proposed⁵ that a second deuterium could be incorporated into the enamine skeleton at C6 (according to the numbering of Figure 1a or C5 according to the numbering used for the intermediates as in Figures 3 and 4). For computational reasons, the double substitution is taken into account only with INMA.

2.5. Sampling Issues. The limited sampling of the configurational space is source of error in the calculation of the Raman spectrum by using both ACF and INMA. To give an estimate of the uncertainty in both position and intensity of the bands, the Raman spectrum for the clavulanate

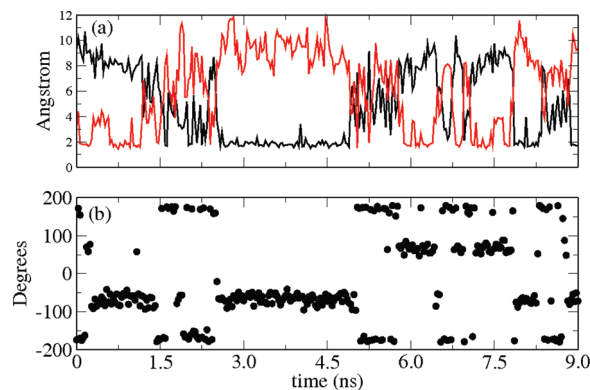


Figure 5. Correlation between the distance between the OH group of the clavulanate intermediate and the Glu240 (black line) and Asp104 (red line) carboxylate oxygens, and the dihedral angle C9-C11-C12-O13 of the clavulanate intermediate. Atom numbering is according to Figure 3.

intermediate was evaluated for the two halves of the QM/MM trajectory. The results are reported as Supporting Information (Figure SI-1). Given the same overall sampling time window, INMA spectra converge faster than those from ACF in that the intensity of only a few bands are affected significantly by the number of configurations taken into account. The same kind of uncertainty is obtained by taking half (16) or, for some modes, a quarter (8) of the INMA points along the entire QM/MM trajectory or taking points on shorter trajectory segments (up to 6 ps). The spectrum calculated from the ACF is more sensitive to the length of the trajectory. This is mainly due to the statistical error on the time ACF. The bands most affected are those at 1590, 1280, and 1160 cm^{-1} , for which variations as high as 25% are observed between the spectrum calculated over the entire simulation and the 12 ps trajectory segments. However, the general shape of the spectrum, in particular the relative intensity of the bands, does not change taking a shorter trajectory. Unacceptable differences among spectra appear when only 6 ps-long trajectory segments are employed for the calculation of the polarizability ACF. On the basis of these considerations, we expect that the intensities of QM/MM spectrum calculated for the tazobactam intermediate, which has been evaluated from a 10-ps long trajectory, might be affected by a larger error than 25%.

3. Results and Discussion

3.1. General Structural Properties. The intermediate from tazobactam is mostly rigid. No conformational changes were observed during the classical and QM/MM simulations. A different situation is observed for the intermediate from clavulanate, where the dihedral angle C9-C11-C12-O13 at the tail of the intermediate chain oscillates between three average values, -70 and $+70$ and $+180$ degrees. These values correspond to three different conformations in which the terminal OH group of the clavulanate intermediate forms a hydrogen bond either with the carboxylate of Asp104 (-70 degrees), or with the carboxylate of Glu240 ($+70$ degrees), or with water (180 degrees). In Figure 5 the correlation between the variation of the distances between the clavulanate OH and the carboxylate groups of Glu240 and Asp104

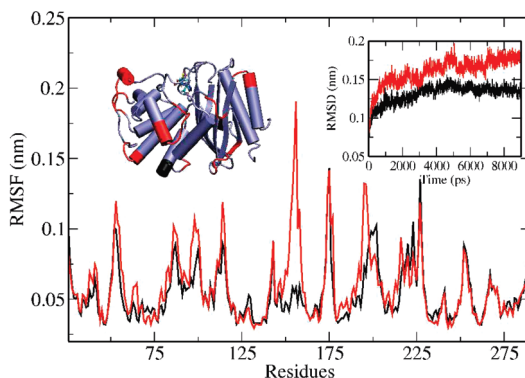


Figure 6. Root mean square fluctuations of the protein residues α carbons for E166A SHV tazobactam (black line) and E166A SHV clavulanate complexes (red line), together with the corresponding RMSF for the two proteins. In the inset regions with higher mobility are highlighted in red and black for clavulanate and tazobactam intermediate protein structure, respectively.

is reported, along with the corresponding value of the dihedral C9-C11-C12-O13. The dihedral angle corresponding to the more stable configuration seems to be that forming a hydrogen bond with Asp104. In fact, the carboxylate of Asp104 is constrained due to another hydrogen bond with the HEPES molecule, whereas that of Glu240 can freely rotate. This is also the conformer that features the smallest root-mean-square displacement of main chain heavy atoms from the crystallographic structure (0.32 ± 0.26 Å compared with 0.53 ± 0.31 Å and 0.59 ± 0.29 Å of the other two conformations). For this reason, as starting point of our QM/MM simulation of the clavulanate intermediate, we chose a configuration in which the OH of the clavulanate intermediate forms an hydrogen bond with the Asp104 residue. We remark that the larger backbone rigidity in the tazobactam intermediate is likely due to the presence of the carboxylate group and the bulky triazole moiety.

The higher mobility of the clavulanate intermediate slightly affects the flexibility of some regions of the protein. This is shown in Figure 6 in which the root-mean-square fluctuations (RMSF) of the C_α for the residues of the E166A SHV clavulanate intermediate (red curve) and tazobactam intermediate (black curve) complexes are reported, together with the corresponding rmsd taken along the 9 ns classical MD trajectories. The regions that present a higher RMSF for the C_α are residues located in loops and helices far from the active site (inset of Figure 6).

Finally, it is worth pointing out that the trans-enamine $O=C-C=C-NH-$ moiety is nearly planar in the intermediate from clavulanic acid, whereas it deviates appreciably from planarity in the intermediate from tazobactam. The dihedral angle around the C=C bond calculated from the QM/MM simulations is $180^\circ \pm 9^\circ$ and $173^\circ \pm 8^\circ$ for clavulanate and tazobactam intermediates, respectively (in the X-ray structure the same angle amounts at 180° and 168°).

3.2. Raman Spectra. In this section the calculated Raman spectrum of the E166A SHV trans-enamine intermediate

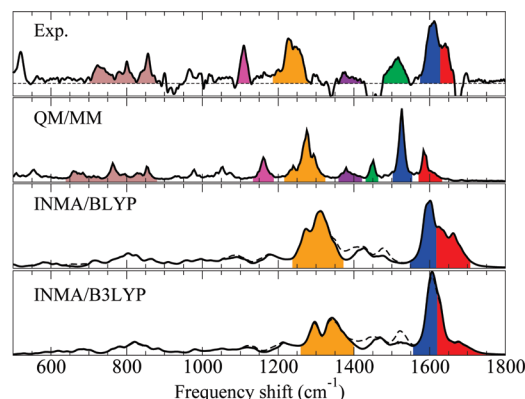


Figure 7. Experimental (ref 1), QM/MM, and INMA (BLYP and B3LYP, see text) Raman spectra for the *h*-clavulanate intermediate bound to the E166A SHV β -lactamase. The experimental data refer to the [protein + inhibitor] – [protein] difference spectrum (the dashed line indicates the zero intensity axis). Band colors indicate the correspondence between calculated and experimental bands based on the theoretical assignment. For INMA the spectrum calculated with (dashed line) and without (solid line) the contribution due to the methyl capping group of the QM subsystem are reported. Intensity in arbitrary units.

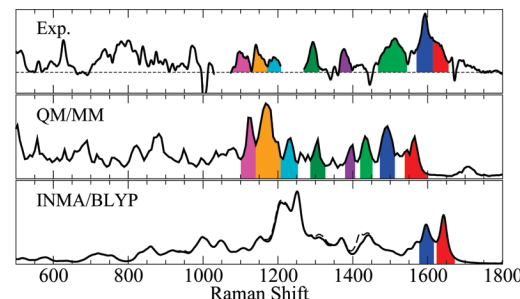


Figure 8. Experimental (ref 1), QM/MM, and INMA Raman spectra for the *h*-tazobactam intermediate bound to the E166A SHV β -lactamase. See also the caption to Figure 7.

from clavulanic acid and tazobactam will be discussed, and an interpretation of the main experimental features will be given.

3.2.1. General Spectral Features. The difference Raman spectrum for the two intermediates is reported in Figures 7 and 8. The spectral region of interest is the one below 1800 cm⁻¹. This region contains many peaks of varying intensities, many of which are not easily identifiable. We recall that positive bands in the [protein + inhibitor] – [protein] difference spectra reflect the [protein + inhibitor] state during or after the inhibition reaction, whereas negative bands are characteristic of the initial [protein] state.

The difference spectra are characterized by a high frequency band structure (around 1600 cm⁻¹) and by a broadband immediately lower in frequency (at 1515 cm⁻¹ and 1512 cm⁻¹ for clavulanate and tazobactam, respectively). The high frequency structure results from the overlap of two bands (at 1605 cm⁻¹ and 1643 cm⁻¹ for clavulanate and at 1595 cm⁻¹ and 1630 cm⁻¹ for tazobactam). In both cases, the band at around 1600 cm⁻¹ has been taken as the signature of the enamine species. The band is slightly red-shifted upon NH deuterium exchange (1587 cm⁻¹ for *d*-clavulanate and

1582 cm⁻¹ for *d*-tazobactam). In addition, the band at 1510 cm⁻¹ disappears upon deuterium exchange. The difference spectrum recorded for sulbactam (not considered in the present study) also reports these features.

The spectra calculated within the QM/MM ACF formalism feature the same number of positive bands as the experimental spectra with approximately the same relative intensity (Figures 7 and 8). This allows us to make a one-to-one correspondence between calculated and experimental bands as shown in the figures. As can be noticed immediately, the three high frequency bands are largely red-shifted with respect to the recorded spectra. In addition, the relative splitting of the bands is larger in the simulated QM/MM spectra. The position of these bands in the recorded trans-enamine clavulanate intermediate is at higher frequency than for tazobactam. This feature is reproduced by the calculated spectra even though the difference between clavulanate and tazobactam bands is more pronounced.

The Raman spectra simulated from the ACF-protocol are also able to reproduce the band structure between 1100 cm⁻¹ and 1300 cm⁻¹ although, in contrast to the high frequency modes, the calculated frequencies are shifted to the blue. In contrast, the spectra calculated from INMA on top of the QM/MM trajectory (Figures 7 and 8) only reproduce a few experimental features well, namely the high frequency bands (above 1580 cm⁻¹) and the large band structure around 1250 cm⁻¹. Other bands are very weak and not easily discernible. In particular the experimental band around 1510 cm⁻¹ is either extremely weak or not present at all.

One of the most serious limitations of INMA is the harmonic approximation on which the method relies. On the other hand, the QM/MM spectrum calculated from the ACF fully takes into account both mechanical and electrical anharmonicity. The only limitation is imposed by the underlying potential energy surface and, in particular, by the exchange and correlation functional employed, i.e., the BLYP exchange and correlation functional.^{23,24} This problem clearly affects in the same measure the QM/MM and the INMA spectra. It is well known that the BLYP functional generally underestimates harmonic vibrational frequencies (see for example ref 39). On the other hand, this functional has been proved to correctly reproduce the anharmonic effects in organic molecules.³⁹ As can be noticed from Figures 7 and 8, QM/MM and INMA frequencies are quite different. In particular INMA seems to overestimate the frequency of modes in the 1580–1000 cm⁻¹ region with respect to both QM/MM and experiment. In addition, as already mentioned, in the QM/MM Raman spectra calculated within the ACF formalism, vibrational frequencies in the interval 1100–1300 cm⁻¹ are also blue-shifted (Figures 7 and 8). Overall, this is in contrast with general deficiencies of the BLYP functional just mentioned. It is deemed therefore necessary to assess the overall reliability of BLYP functional for the present system. To this end, the INMA spectrum for the intermediate from clavulanic acid was also calculated employing the B3LYP functional,¹⁴ which performs well in vibrational calculations.³⁹ In Figure 7 the INMA spectra calculated with the two exchange and correlation functionals is shown (see also Table 3 where the detailed information about some

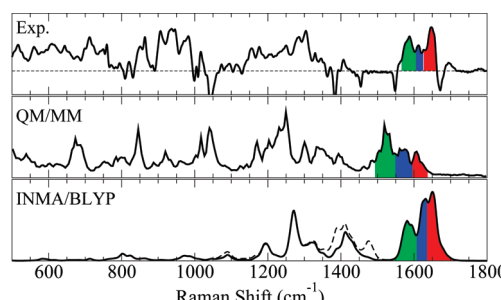


Figure 9. Experimental (ref 1), QM/MM, and INMA Raman spectra for the *d*-clavulanate intermediate bound to the E166A SHV β -lactamase. See also the caption to Figure 7.

vibrational mode is reported; the assignment of the Raman bands is discussed in the next section). As can be seen, in our specific case, when averaging over many configurations, the differences between the two functionals do not appear to be relevant. The observed frequency blue shift could be a result of the embedding empirical force field. In a previous work on clavulanic acid in aqueous solution,⁷ no appreciable frequency differences were reported between QM/MM and full QM frequency calculation. However, in the present case the effect on the vibrational properties of the (highly isotropic) embedding potential is difficult to predict *a priori*. The difference in the shift of the high frequency bands between QM/MM ACF and INMA spectra can be explained in terms of anharmonicity as discussed in Section 3.2.2.

Upon isotopic NH \leftrightarrow ND exchange, the broad band at about 1515 cm⁻¹ disappears. The calculated QM/MM spectra of the deuterated clavulanate trans-enamine also lacks the 1450 cm⁻¹ peak (Figure 9b). The experimental clavulanate spectrum in D₂O reports also the separation of the two overlapping bands between 1570 cm⁻¹ and 1670 cm⁻¹ into three quite well resolved bands. This feature is also nicely reproduced by the calculated QM/MM spectrum for *d*-clavulanate (Figure 9b). We remark that the high frequency band is located near the amide I band of the unbound enzyme (negative band at 1670 cm⁻¹). In general, the enamine spectrum of clavulanate is more difficult to obtain because the enamine peaks are broader and overlap to a greater extent with the protein amide I band, which is subtracted away to generate the difference spectra. The residual amide I band intensity, which is present in both *d*- and *h*-clavulanate spectra, is likely due to small conformational changes in the protein on acylation of Ser70 residue or incomplete subtraction of the protein in the difference spectra. For these reasons, the positive band at 1648 cm⁻¹ cannot be unambiguously assigned to the intermediate. The main difference between the calculated spectra for *h*- and *d*-tazobactam is the disappearance of the band at 1540 cm⁻¹ (Figure 10b).

Further comparison with the experimental spectra of the deuterated trans-enamine intermediates is made problematic because of additional features, which appear in the difference spectra because of the difficulty of subtracting to zero intense peaks that are due to the buffer and the protein. In addition, to prepare the protein crystals in deuterated buffer, the crystals are removed from the mother liquor solution and undergo soaking for 24 h in advance of the Raman experi-

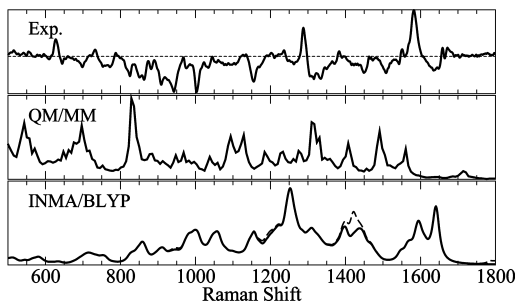


Figure 10. Experimental (ref 1), QM/MM, and INMA Raman spectra for the *d*-tazobactam intermediate bound to the E166A SHV β -lactamase. See also the caption to Figure 7.

ment to ensure H \leftrightarrow D exchange. This also influences the quality of the Raman difference spectra, introducing more noise.

We finally remark that, compared to experiments, the calculated QM/MM spectra feature narrower bands. This could be due to differences in temperature between experiments and numerical simulations. Indeed, the specimen temperature at the laser spot might be as high as 40 °C compared to room temperature at which simulations are carried out.

3.2.2. Vibrational Assignment. The assignment of vibrational spectra of large molecular assemblies represents a major problem. To this end, several methods have been proposed in the literature (see for instance refs 7, 8, 10, 40, and 41). In the present work a quantitative assignment has been performed using the vibrational density of states (VDOS), as obtained from the power spectrum of the velocity-velocity time autocorrelation functions, projected along the “quasi-harmonic” vibrational modes calculated from INMA. As discussed in a previous publication,⁷ many INMA eigenvectors are a good representation of a given vibrational mode at finite temperature. Indeed, INMA modes do not lose their character appreciably as a consequence of anharmonicity, giving rise to sharp single peak spectral features when used to project atomic velocities (Figure 11). Instead, some other modes are strongly mixed up by anharmonicity. This is particularly relevant for modes localized on very flexible parts of the trans-enamine intermediates. For this reason, using this projection procedure, it is difficult to assign the low frequency modes (<1000 cm⁻¹). However, this spectral region is not necessary to gain an understanding of the inhibitor/lactamase reaction mechanism. Overall, even though in the present case INMA does not seem to reproduce the overall Raman spectrum as well as the QM/MM simulation, the eigenmodes that are obtained represent a good basis set for band assignment. In Figure 11 some examples of projections for modes above 1100 cm⁻¹ are reported for the clavulanate intermediate.

The projection procedure allows us to assign several important bands of the Raman spectra. In Tables 1 and 2 the results of this analysis are summarized for clavulanate and tazobactam, respectively. Although many instant normal modes conserve their identity during the intermediate dynamics, their vibrational frequencies largely differ from the harmonic one. In particular the vibrational modes between 1580 and 1700 cm⁻¹ are downshifted systematically in the

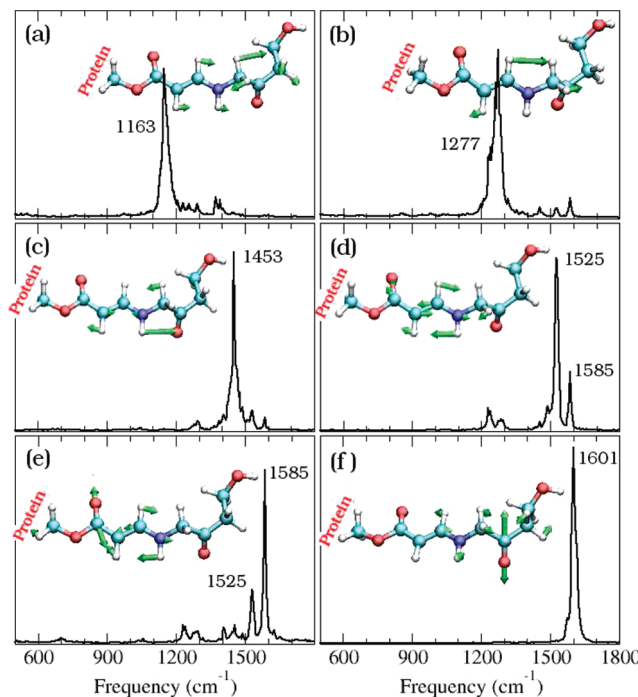


Figure 11. Vibrational density of states projected along a given Raman active (instant normal) mode obtained from the INMA. In each panel, the corresponding normal mode is shown with green arrows (only atomic components larger than a cutoff value $c = 0.1$ are reported). Intensity in arbitrary units. The calculation has been performed projecting velocities on atoms with eigenmode components greater than c . Each molecular dynamics frame has been roto-translated in a such a way to minimize the root-mean-square deviation from the configuration employed in the INMA analysis (only the atoms used for the projection have been considered in the minimization).

QM/MM simulation. This is not a consequence of the different computational framework used for the QM/MM simulation (pseudopotentials for the core functions and plane waves up to 70 Ry for the valence electrons) and the INMA (all-electron calculations with a triple- ζ cc-VTZ basis set). Indeed the harmonic frequencies of small model molecules (acetone, ethylene, and N-methyl enamine) calculated with the two methods barely differ (differences within 10 cm⁻¹). Therefore, discrepancies are likely due to anharmonicity, which is not taken into account in the INMA. For this reason the better accord between INMA and experiment in the frequency range from 1590 cm⁻¹ to 1650 cm⁻¹ should be considered fortuitous.

In the following, the vibrational assignment is discussed for the region from 1000 cm⁻¹ to 1800 cm⁻¹ and in particular for the region from 1500 cm⁻¹ to 1800 cm⁻¹, which has been proved critical for the understanding of the nature of the SHV reaction intermediate. The intermediate from clavulanic acid and tazobactam will be discussed in parallel as much as possible since they present common spectral features due to the enamine moiety.

Enamine Related Modes. The two experimental bands around 1600 cm⁻¹ and 1640 cm⁻¹ in the experimental spectra are unambiguously assigned to the C³=O⁴/C⁵=C⁶ symmetric (1640 cm⁻¹) and asymmetric stretching (1600 cm⁻¹) strongly

Table 1. Vibrational Analysis for *h*- and *d*-Clavulanate Bound to E166A- β Lactamase^a

<i>h</i> -clavulanate				<i>d</i> -clavulanate				assignment
INMA			INMA			freq	int	assignment
QM/MM freq	freq	int	exp. freq	QM/MM freq	freq			
978	999(8)	2(2)		968	988(8)	3(2)		out-of-plane CH=CH-NH X-H atom wagging
1057*	1071(17)	5(3)		1021	1039(21)	5(2)		mostly C ⁸ -N ⁷ strctch
1075*	1100(28)	9(7)		1045	1086(11)	8(5)		C ⁵ -H in-plane rocking and C ⁸ H ₂ , C ¹¹ H ₂ twisting
1160*	1179(12)	9(5)		1171	1185(11)	8(5)	1105	mostly C ⁸ H ₂ twisting
1163*	1187(13)	6(4)		1179	1192(13)	6(5)	1105	coupled C ¹¹ H ₂ and C ¹² H ₂ twisting
1240*	1299(15)	18(15)		1234	1299(15)	15(14)	1202	mostly C ¹¹ H ₂ wagging and C ¹² H ₂ twisting
1277*	1310(13)	25(23)	1230	1250	1312(15)	6(5)	1230	in-plane, in-phase enamine CH=CH-NH-CH ₂ H-atoms rocking
1296*	1321(20)	18(17)	1295	1301	1321(20)	18(17)	1250	in-plane enamine CH=CH-N-CH ₂ H atoms rocking
1380*	1417(16)	17(5)		1387	1416(16)	18(10)		C ⁸ H ₂ scissoring
1393*	1422(13)	10(4)		1401	1424(8)	11(5)		C ¹¹ H ₂ scissoring
1410*	1465(11)	10(2)		1427	1465(11)	9(1)		C ¹² H ₂ scissoring
1450	1540(36)	3(1)		1447	1567(33)	5(4)		O ¹³ -H wagging
1453*	1511(15)	10(3)	1515	995	986(6)	4(3)		N ⁷ -H rocking (no activity for <i>d</i> -clavulanate)
1530*	1602(12)	76(22)	1605	1523	1586(15)	46(19)	1592	coupled symmetric C ³ =O ⁴ ; C ⁵ =C ⁶ stretching and C ⁶ -H; N ⁷ -H rocking
1588*	1652(18)	29(16)	1643	1570	1642(12)	40(22)	1613	coupled asymmetric C ³ =O ⁴ ; C ⁵ =C ⁶ stretching and C ⁶ -H; N ⁷ -H rocking
1605*	1682(17)	17(8)	—	1605	1682(16)	16(7)	1648	C ⁹ =O ¹⁰ stretching
1323	1089(11)	5(2)						CH ₃ capping group bending
1410	1385(12)	13(8)						CH ₃ capping group twisting
1415	1390(11)	13(10)						CH ₃ capping group umbrella
1730	1479(9)	16(3)						CH ₃ capping group bending

^a For instant normal mode analysis (BLYP/cc-pVTZ level), INMA, the average frequency and the Raman scattering activity (Int) are also given (standard deviations in parentheses). Frequencies in cm⁻¹ and Raman activities in Å⁴/a.m.u. QM/MM-Raman active modes are labeled with a dot (*). Atom numbering is according to Figure 3.

Table 2. Calculated and Experimental Raman Spectrum for *h*- and *d*-Tazobactam Bound to E166A- β Lactamase^a

<i>h</i> -tazobactam				<i>d</i> -tazobactam				assignment
INMA			INMA			QM/MM freq	freq	assignment
QM/MM freq	freq	int	exp. freq	QM/MM freq	freq	int	exp. freq	
848	828(18)	2(3)		838	839(17)	1(3)		triazole C ¹⁸ -H, C ¹⁹ -H asymm. wagging
882*	931(37)	12(5)		882	934(19)	9(6)		S ¹¹ O ₂ symmetric stretching
925	993(6)	15(9)		930	992(12)	18(11)		S ¹¹ O ₂ asymmetric stretching
1125*	1206(16)	31(25)	1100	1128	1208(11)	34(20)		triazole N ¹⁵ =N ¹⁶ =N ¹⁷ asymm. stretching
1170*	1210(10)	66(23)	1143	1095	1163(26)	25(10)		in-plane, out-of-phase C ⁵ -H, N ⁷ -H rocking
1200*	1247(12)	73(37)		1200	1225(12)	20(12)		mostly C ⁸ -H bending
1275*	1234(15)	40(29)	1290	1269	1249(10)	79(26)		triazole breathing mode
1285*	1337(11)	7(3)		1280	1333(15)	11(7)		in-plane, in-phase C ⁶ -H and C ⁸ -H rocking
1292*	1282(9)	15(13)		1231	1279(13)	19(11)		C ²⁰ O ₂ carboxyl symmetric stretching
1304*	1374(9)	6(3)	(1290)	1316	1395(9)	41(16)		in-plane, enamine CH=CH-N-CH ₂ H atoms rocking
1348*	1368(10)	31(11)		1353	1373(11)	11(10)		C ¹⁰ H ₃ umbrella
1355*	1419(7)	14(9)		1348	1418(6)	14(8)		triazole N ¹⁵ =C ¹⁹ stretching
1398*	1442(7)	30(15)	1378		1442(7)	30(15)		C ¹⁰ H ₃ and C ¹⁴ H ₂ scissoring
1402	1409(4)	12(8)		1405	1456(9)	7(5)		C ¹⁰ H ₃ scissoring
1409	1457(9)	7(4)		1406	1457(9)	7(4)		triazole C ¹⁸ =C ¹⁹ stretching
1435*	1495(19)	21(12)	1512	(990)	1040(12)	6(3)		N ⁷ -H rocking (no activity for <i>d</i> -tazobactam)
1488	1594(16)	10(8)		1488	1595(22)	12(18)		C ²⁰ O ₂ carboxyl asymmetric stretching coupled to the C ⁸ -H wagging
1498*	1607(21)	49(44)	1595	1486	1581(18)	33(25)	1583	coupled symmetric C ³ =O ⁴ ; C ⁵ =C ⁶ stretching and C ⁶ -H; N ⁷ -H rocking
1562*	1629(21)	78(50)	1630	1548	1617(15)	69(59)		coupled asymmetric C ³ =O ⁴ ; C ⁵ =C ⁶ stretching and C ⁶ -H; N ⁷ -H rocking
1155	938(10)	4(3)						CH ₃ capping group bending
1260	1194(8)	13(10)						CH ₃ capping group twisting
1418	1349(7)	29(20)						CH ₃ capping group umbrella
1716*	1289(14)	11(6)						CH ₃ capping group bending

^a For instant normal mode analysis (BLYP/cc-pVTZ level), INMA, the average frequency and the Raman scattering activity (Int) are also given (standard deviations in parentheses). Frequencies in cm⁻¹ and Raman activity in Å⁴/a.m.u. QM/MM-Raman active modes are labeled with a dot (*). Atom numbering is according to Figure 4.

coupled with the C⁶-H/N⁷-H in-plane rocking (Figure 11d,e). These delocalized stretching/rocking modes are commonly referred to as O=C-C=C=NH— enamine backbone stretching.¹ In the QM/MM spectra, these two modes fall at 1530 cm⁻¹ and 1588 cm⁻¹ for clavulanate and

1488 cm⁻¹ and 1498 cm⁻¹ for tazobactam. These modes also have strong Raman activity according the INMA even though, as already remarked, they are higher in frequency and less separated (1601 cm⁻¹ and 1647 cm⁻¹ for clavulanate and 1607 cm⁻¹ and 1627 cm⁻¹ for tazobactam).

Table 3. Instant Normal Mode Analysis of the Effect of Isotopic Substitution on Some Stretching Vibrational Modes of SHV Reaction Intermediates from Clavulanic Acid and Tazobactam^a

asymm. (CO_2)		asymm. ($\text{O}=\text{C}-\text{C}=\text{C}-\text{NH}-$)		symm. ($\text{O}=\text{C}-\text{C}=\text{C}-\text{NH}-$)		C=O	
freq	int	freq	int	freq	int	freq	int
Clavulanate BLYP							
0d		1602(12)		76(22)		1652(18)	
1d		1586(15)		46(19)		1642(12)	
2d		1581(16)		36(15)		1636(13)	
Clavulanate B3LYP							
0d		1610(11)		109(27)		1675(14)	
1d		1593(13)		87(23)		1655(12)	
2d		1588(13)		77(24)		1647(13)	
Tazobactam BLYP							
0d	1594(16)	10(8)	1607(21)	49(44)		1629(21)	77(51)
1d	1595(22)	12(18)	1581(18)	63(48)		1617(15)	69(53)
2d	1593(14)	19(21)	1576(16)	53(48)		1616(17)	80(54)

^a Average frequency and the Raman scattering activity (Int) at BLYP/cc-pVTZ and B3LYP/cc-pVTZ level for normal (0d), singly deuterated at N7 (1d), and doubly deuterated at N7 and C5 (2d) intermediates are reported (standard deviations in parentheses). Frequencies in cm^{-1} and Raman activity in $\text{\AA}^4/\text{a.m.u.}$ Atom numbering is according to Figures 3 and 4.

In the QM/MM Raman spectrum of (singly deuterated) *d*-clavulanate, these two bands resolve into three overlapping peaks. Of these, the two peaks at lower frequency are assigned to the delocalized trans-enamine stretching and rocking mode. The highest frequency band instead is due to the pure enamine $\text{C}^9=\text{O}^{10}$ vibration (Figure 11f). This mode does not undergo any frequency shift upon isotopic exchange, and it might be responsible for the high frequency shoulder of the 1588 cm^{-1} band in the *h*-clavulanate spectrum. We point out that the $\text{C}^9=\text{O}^{10}$ stretching presents an appreciable Raman activity also in the INMA (Table 1). The experimental spectrum of *d*-clavulanate also displays three bands. The one at high frequency (around 1650 cm^{-1}) is however doubtful as it is located near a possible protein amide I band subtraction artifact. In addition, its position is quite anomalous for a ketonic group being about 60 cm^{-1} lower than the typical frequency of a saturated ketone C=O stretch. Nevertheless, the C=O mode has generally an appreciable Raman activity, and a signal due to it should be expected in the spectrum. However, no bands are present in the experimental spectrum of both *h*- and *d*-clavulanate in the $1700\text{--}1800 \text{ cm}^{-1}$ interval. For this reason, the possibility of a large redshift for the C=O stretching frequency was investigated. Several reasons can be envisaged for the large redshift of the CO band. It has been reported in literature that hydrogen bonding and the environment electric field have a bathochromic effect on the C=O stretch.^{42–44} In the present case, the $\text{C}^9=\text{O}^{10}$ group is found to be hydrogen-bonded to 1.1 ± 0.7 water molecules and to the Asn¹⁷⁰ side chain. In a first attempt to elucidate the role of these hydrogen bonds and of the electrostatic field of the protein and the aqueous medium generally, INMA was carried out in the absence of the classical point charges. The resulting C=O frequency was blue-shifted by about 35 cm^{-1} . To further address this point, the electronic structure of the carbonyl group was characterized in terms of localized Boys orbitals⁴⁵ (BO) corresponding to covalent bonds and lone pairs. The center of charge of the BOs (BOC) provides a useful tool to quantify the polarization of covalent bonds and to analyze differences in the electronic structure of the same functional group in different environments.⁴⁶ The electronic structure

of the intermediate in the enzyme pocket for 20 equispaced in time configurations was compared with that calculated, for the same configurations, in the absence of the environment electric field. In the first case, the BOC of the C=O double bond is located at $0.676 \pm 0.004 \text{ \AA}$ from the carbon atom, whereas in the latter this distance is $0.657 \pm 0.004 \text{ \AA}$, very close to that in acetone in vacuo (0.656 \AA). This sizable polarization of the carbonyl charge density is indicative of a larger weight of the carbonyl single-bond C^+-O^- Lewis resonance structure to C=O bond and implies a reduction of the stretching vibrational frequency. This finding supports the idea that a shift of the intermediate C=O backbone frequency to the region of the amide I band is plausible, and it strongly supports the proposal that the experimental feature at 1650 cm^{-1} is not an artifact but due to the C=O vibration.

We also point out that the symmetric and asymmetric enamine stretch modes can also account for the bands recently observed at 1595 cm^{-1} and 1658 cm^{-1} in the spectrum of the tazobactam intermediate from the wildtype SHV enzyme.⁵ On the basis of a vibrational analysis on minimal models of possible reaction intermediates in the gas phase,⁵ the latter was assigned to the $\text{N}=\text{H}^+$ of an immine species coexisting with the trans-enamine intermediate (Figure 1). Our calculations suggest that the trans-enamine species also can explain this band.

Enamine Related H Rocking Bands. The experimental band around 1515 cm^{-1} can be unambiguously attributed to the enamine N⁷–H in-plane rocking (Figure 11c). Indeed, this is the only vibrational mode below the enamine asymmetric stretching band common to both clavulanate and tazobactam intermediates. In the QM/MM spectra this mode is located at 1453 cm^{-1} for clavulanate and 1435 cm^{-1} for tazobactam and possesses a very large Raman scattering activity. However, the bandwidth in the QM/MM spectrum is considerably narrower than the experimental one. The INMA predicts little Raman scattering activity for this mode (in particular for the intermediate from clavulanate), but its frequency is more consistent with the experiment (1511 cm^{-1} and 1495 cm^{-1} for clavulanate and tazobactam, respectively). In the singly deuterated trans-enamine the N–H rocking

vibration remarkably downshifts at around 1000 cm^{-1} and does not show any appreciable Raman activity in either the QM/MM or the INMA spectra.

The enamine N–H rocking motion also gives rise to other bands in the Raman spectrum. In particular in the clavulanate intermediate the very intense band at 1277 cm^{-1} is mostly due to the in-plane, in-phase rocking motion of the H atoms of the $\text{C}^5\text{H}=\text{C}^6\text{H}-\text{N}^7\text{H}-\text{C}^8\text{H}_2$ fragment (Figure 11b). This band nicely correlates with the very intense peak at 1230 cm^{-1} in the recorded spectrum. The mode slightly redshifts upon deuterium substitution.

A similar vibrational mode has not been found in the tazobactam intermediate, likely because of the perturbation introduced by the bulky groups at C^8 . Rather a coupled $\text{C}^5-\text{H}/\text{N}^7-\text{H}$ mode gives rise to the very intense band at 1170 cm^{-1} , which correlates to the experimental band at 1100 cm^{-1} . Because of the large N–H contribution to this mode, the band downshifts of about 75 cm^{-1} in the deuterated QM/MM spectrum.

Finally, we remark that the experimental spectra of both inhibitors in aqueous solution and enzyme reaction intermediates present a band around 1290 cm^{-1} .¹ Tazobactam and the tazobactam intermediate feature a sharper and more intense band. In a previous study,⁷ the (broad) 1290 cm^{-1} band in the QM/MM spectrum of clavulanic acid in water was assigned (mostly) to the lactam ring C–H rocking mode (C^4-H according to Figure 1a numbering). The present theoretical analysis of the clavulanate and tazobactam reaction intermediates suggests that the C^5-H and C^6-H (which corresponds to the lactam ring C–H of the unreacted inhibitor) in-plane rocking mode has also an appreciable Raman scattering section and gives rise to a band around 1300 cm^{-1} . The unique assignment of the experimental feature around 1290 cm^{-1} band to the lactam or enamine C–H moiety is made problematic by the presence in this region of a triazolyl moiety mode.⁵ This point is further addressed when discussing tazobactam specific vibrational modes.

Clavulanate Specific Bands. The intermediate from clavulanic acid has three aliphatic CH_2 groups, which give rise to Raman activity in the QM/MM spectrum. The CH_2 scissoring modes originate the weak band at 1390 cm^{-1} , which correlates with the equally weak structure at 1375 cm^{-1} in the experimental difference spectrum. INMA also predicts Raman activity for the CH_2 scissoring modes.

In contrast CH_2 twisting modes show high activity in the QM/MM spectrum and are responsible for the intense band at around 1160 cm^{-1} , which we assign to the intense peak at 1105 cm^{-1} in the experimental spectrum. In addition, the C^{12}H_2 twisting coupled with the C^{11}H_2 scissoring gives rise to the peak at 1240 cm^{-1} to the left of the intense 1277 cm^{-1} band.

The modes so far discussed complete the band assignments of the QM/MM Raman spectrum of the enamine intermediate from clavulanic acid and provide a satisfactory interpretation of the experimental Raman spectrum between 1000 cm^{-1} and 1700 cm^{-1} .

Tazobactam Specific Bands. The intermediate from tazobactam has a more complex structure than that of clavulanate.

The most relevant differences are the presence of the triazole ring, the carboxylate group, and the sulfoxo group. These groups make the tazobactam Raman spectrum very rich.

Among all of the vibrational modes localized on the triazole ring only three present an appreciable Raman activity both in QM/MM and INMA above 1000 cm^{-1} . The first is the $\text{N}^{15}=\text{N}^{16}=\text{N}^{17}$ asymmetric stretching, which produces the band at 1125 cm^{-1} . This mode correlates well with the experimental band at 1100 cm^{-1} , even though its intensity is higher than the experimental one. The second Raman active mode is a triazolyl breathing-like mode (1275 cm^{-1} and 1234 cm^{-1} according the QM/MM simulation and the INMA, respectively). Its calculated QM/MM Raman scattering section is however little while quite large at the INMA level. The third active triazole mode is the $\text{N}^{15}=\text{C}^{19}$ stretching, which gives rise to the band at 1353 cm^{-1} . However its Raman activity is doubtful as it overlaps with the C^{10}H_3 umbrella motion at 1355 cm^{-1} .

In a recent investigation of the trans-enamine intermediate from wildtype SHV β -lactamase, Kalp et al.⁵ proposed that the 1290 cm^{-1} peak is due to the breathing mode of the triazolyl moiety. The present study on the E166A mutant is consistent with this assignment. However, as already discussed, C–H distortions also have a high Raman activity around 1300 cm^{-1} . Therefore, we suggest that both C–H rocking and triazole localized vibrations might both originate the observed band at 1290 cm^{-1} . This proposal explains why the 1290 cm^{-1} band in the intermediate from tazobactam has an intensity higher than that from clavulanic acid. We remark that on the basis of INMA Raman activities only the triazole localized mode could give rise to the 1290 cm^{-1} even though its frequency is considerably smaller than the experimental one.

The carboxylate symmetric stretch gives rise to a band at 1292 cm^{-1} with a weak intensity in the QM/MM spectrum (1326 cm^{-1} in the INMA with low intensity). The asymmetric CO_2 stretch falls at 1488 cm^{-1} , and it is either inactive or its intensity is lower than the background noise. However, in the INMA this mode shows a quite high activity at 1594 cm^{-1} . Kalp et al.,⁵ on the basis of gas-phase models, assigned the observed band at 1630 cm^{-1} in the spectrum of tazobactam intermediate from the wildtype SHV enzyme to the asymmetric CO_2 stretch. In their model, which lacks the triazolyl moiety and the sulfoxo group, the asymmetric CO_2 is strongly coupled to the enamine $\text{O}=\text{C}=\text{C}=\text{NH}$ –stretch, and its frequency down shifts upon NH/ND exchange according to observed behavior of the experimental band. However, according to our analysis, no such coupling between CO_2 symmetric stretch and enamine stretch is found, and, consequently, no appreciable isotopic effect is observed for the CO_2 stretch both in QM/MM and INMA spectra. The small structural differences between the wildtype enzyme and the E166A mutant here studied might suppress any coupling between the CO_2 symmetric stretch and enamine stretch observed for the gas-phase model. Our results suggest that the 1630 cm^{-1} in the wildtype SHV intermediate is due to some other species. Indeed, in light of the discussion about the enamine related modes above, a plausible candidate for the 1630 cm^{-1} is the imine intermediate (Figure 1).

The sulfone group stretching modes are strongly coupled with other stretching and bending modes all over the intermediates. The symmetric stretch gives rise to a moderately intense band at 882 cm^{-1} in the QM/MM, whereas the asymmetric mode (925 cm^{-1}) does not have any detectable Raman activity. In contrast, INMA predicts both modes to have an appreciable activity.

Finally, a vibrational mode due to the C^{10}H_3 and C^{14}H_2 scissoring unambiguously originates the band at 1398 cm^{-1} in the QM/MM. INMA predicts also a high activity for this mode. This completes the assignment of the Raman vibrational spectrum for the intermediate from tazobactam.

Comments on Isotopic H/D Exchange. In a recent report, it has been proposed that two deuterium atoms are incorporated into the enamine skeleton.⁵ Indeed, on the basis of a vibrational (harmonic) analysis of a minimal model of the trans-enamine intermediate in the gas-phase,⁵ the single enamine NH/ND exchange cannot explain the observed down shifts of the enamine $\text{O}=\text{C}-\text{C}=\text{C}-\text{NH}-$ (symmetric) stretching at 1595 cm^{-1} in the tazobactam intermediate from wildtype SHV. These calculations show that only when deuterium is included at C5 of the single intermediate skeleton (C6 of the lactam ring, Figure 1a) the enamine stretching shifts down in accord to experiments. In contrast, our vibrational analysis, carried out on the E166A SHV taking into account the entire intermediate and the coupling with the environment (protein and aqueous medium), indicates that the single NH/ND is sufficient to explain the observed isotopic shift. Indeed, the INMA results reported in Table 3 suggest that the C5 substitution does not induce any further appreciable frequency shift.

The discrepancies between the present calculations and those reported in ref 5 might be attributed to a reduced C^5-H rocking character and an increased N–H rocking character of the coupled $\text{O}=\text{C}-\text{C}=\text{C}-\text{NH}-$ trans-enamine symmetric stretching/H-rocking mode when passing from the minimal model to the full atomistic description of the intermediate at finite temperature (the ratio between the C^5-H and N–H characters goes from 14.0 to 0.2).

3.3. Effect of the Environmental Electric Field. The electrostatic field of the protein frame and the surrounding solution to which the trans-enamine is partially exposed obviously influence both frequency and Raman activity of the vibrational modes. We already mentioned how the environmental electrostatic field polarizes the $\text{C}^9=\text{O}^{10}$ carbonyl group of the intermediate from clavulanic acid, causing a redshift toward the amide I region. In this section we analyze in detail the role of the electrostatic embedding on the Raman spectrum. For computational reasons, we have focused our attention only on the intermediate from clavulanic acid.

In Figure 12, the spectrum calculated without the environmental electrostatic field is compared to the full spectrum. As expected, the electrostatic polarization of the intermediate due to the surrounding medium influences the intensity of several bands in both QM/MM and INMA spectra.

We will discuss the QM/MM spectrum first. As can be seen from Figure 12, two major bands are activated by the environment field. The first one is the band at 1163 cm^{-1} in

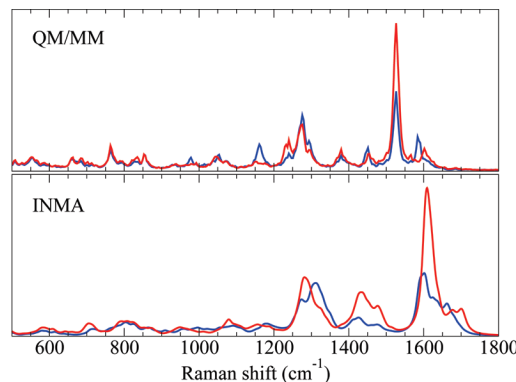


Figure 12. QM/MM and INMA Raman spectra calculated for the clavulanate intermediate with (blue line) and without (red line) the electrostatic fields of the environment. Intensity in arbitrary units.

the QM/MM spectrum, which corresponds to a coupled C^{11}H_2 and C^{12}H_2 twisting. The second and more important band is that at 1588 cm^{-1} , which is due to the asymmetric $\text{C}^3=\text{O}^4/\text{C}^5=\text{C}^6$ stretching coupled to the $\text{C}^6-\text{H}; \text{N}^7-\text{H}$ rocking. Conversely, the Raman intensity of other bands is reduced by the external electrostatic field. Among them, it is of interest to mention the band at 1530 cm^{-1} , which originates from the symmetric $\text{C}^3=\text{O}^4/\text{C}^5=\text{C}^6$ stretching coupled with the $\text{C}^6-\text{H}; \text{N}^7-\text{H}$ rocking and the band at 1600 cm^{-1} due to the $\text{C}^9=\text{O}^{10}$ stretching.

In the INMA spectrum no bands appear to be activated by the environment electrostatic field, which instead considerably reduces the intensity of (i) the CH_2 scissoring bands between 1410 and 1470 cm^{-1} , of (ii) the N–H rocking band at 1511 cm^{-1} , and, as for the QM/MM spectrum, of (iii) the symmetric $\text{C}^3=\text{O}^4/\text{C}^5=\text{C}^6$ stretching band at 1601 cm^{-1} .

Since the time evolution of the polarizability of the intermediate is modulated by the underlying dynamics of atoms, the position of bands in the QM/MM spectrum calculated from the ACF does not shift upon removal of the electrostatic field. This is of course not the case of the INMA spectrum. The larger frequency shift is observed for the three Raman active modes between 1600 cm^{-1} and 1650 cm^{-1} .

The comparison between QM/MM and INMA spectra calculated with and without the embedding electrostatic potential allows us to draw important conclusions on the role of environment modulation of the Raman activity. It is evident from Figure 12 that the mode at 1163 cm^{-1} (CH_2 twisting) is Raman active only in the spectrum calculated from the ACF and only when the (dynamical) modulation by the environment field is taken into account. This modulation is also responsible for the high Raman scattering intensity of the asymmetric $\text{C}^3=\text{O}^4/\text{C}^5=\text{C}^6$ stretching at 1588 cm^{-1} and of the small intensity of the $\text{C}^9=\text{O}^{10}$ stretching.

We finally remark that the INMA Raman activity for some modes show large fluctuations (i.e., high standard deviation from the average, see Tables 1 and 2). This is a consequence of the large change in the local electric field due to the surrounding environment. These changes are very rapid and depend mostly on the nearest coordination shells of the reaction intermediate. The large amplitude field oscillations have a characteristic time of a few picoseconds and average out on a multipicosecond time scale.

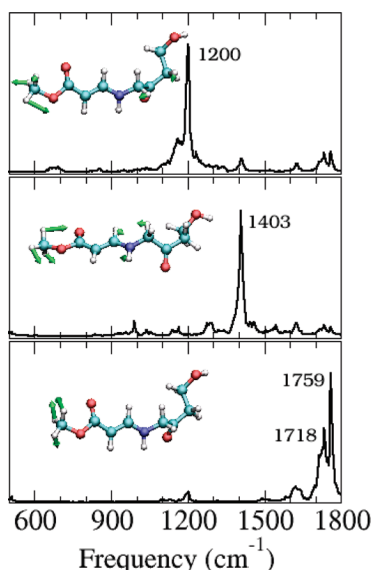


Figure 13. Vibrational density of states projected along three (instant normal) modes localized on the QM capping methyl group. Intensity in arbitrary units.

3.4. Influence of the QM/MM Interface: Effect of the Capping Atoms. The QM models have been built by cutting the inhibitor/protein adducts to the C_β of Ser70 and saturating its valence with an hydrogen atom. The resulting capping methyl group is linked to the MM part via standard bonded force field parameters (stretching, bending, and torsional energy terms). Of course this perturbs the intermediate electronic structure structure and its vibrational properties. In particular, vibrational modes involving the capping methyl group are artificially introduced. These modes might hamper the calculation of the Raman spectrum as they could be Raman active, and they could couple with other modes therefore altering their vibrational frequency. The latter issue cannot be easily addressed, but, in principle, it should be expected that the larger the coupling, the greater the perturbation.

Many INMA vibrational modes have an appreciable component on the capping group. Of these modes, the majority are localized on the methyl group and present, according to INMA, Raman activity in the region between 1300 cm^{-1} and 1500 cm^{-1} (see Figures 7–10 and Tables 1 and 2). In the INMA spectra discussed in the previous section, modes giving rise from this spurious Raman activity are neglected from the analysis. This is not done as easily in the QM/MM spectrum as the time evolution of the polarizability of the reaction intermediate is intrinsically modulated also by the capping group vibrations. However, no Raman activity has been found in the QM/MM spectra for modes localized on the capping group. In fact, as can be seen from Figure 13, in the intermediate from clavulanic acid, vibrational modes of the capping group present sharp spectral signatures when projected onto atomic velocities, and their frequencies do not coincide with any band in the Raman spectrum (Table 1). The same holds for the tazobactam intermediate (Table 2).

In addition, the frequency of these modes is largely blue-shifted with respect to INMA. This is due to the reduced

mobility of the capping hydrogen because of both nonbonded and bonded interactions via the force field. Indeed, these interactions make the confinement potential in which the capping hydrogen is located harder in the QM/MM simulation than that in the INMA. This also reduces the time modulation of polarizability by the motion of the capping hydrogen and therefore the influence on the Raman activity. Only the intermediate from tazobactam has one mode at 1716 cm^{-1} associated with the capping group with appreciable Raman activity (Figures 8 and 10).

4. Conclusions

The vibrational Raman spectra of the trans-enamine intermediate of the E166A SHV β -lactamase inhibition reaction by clavulanic acid and tazobactam, two major clinically available inhibitors, have been calculated from state-of-the-art atomistic calculations. Two methods have been compared: (i) quantum-chemistry harmonic vibrational analysis with temperature averaging included via instant normal-mode analysis (INMA)^{8–10} and (ii) power spectrum of the time autocorrelation function of the polarizability tensor components as obtained from QM/MM simulations. In both cases, the quantum mechanical problem was solved within the same DFT-theory framework. Differences are therefore expected to arise mainly from mechanical (frequencies beyond the second order derivatives of the potential energy) and electrical (band intensity beyond the first derivative of polarizability) anharmonic effects. Spectra calculated within the ACF formalism seem to better correlate with the experimentally recorded spectra as they feature the same number of bands with approximately the same relative intensity. In contrast, INMA seems to reproduce only a few experimental features. In particular, a band attributed to the enamine N–H in-plane rocking has very little Raman activity according to INMA. Other vibrational modes, which are active according to the spectra calculated from ACF, are missing in INMA. Instead, the spectra obtained from the QM/MM simulations allowed us to unambiguously assign the experimental spectra in the region between 1000 cm^{-1} and 1800 cm^{-1} . According to these simulations and consistent also with INMA calculations, the trans-enamine moiety gives rise to a $\text{C}^3=\text{O}^4/\text{C}^5=\text{C}^6$ symmetric and asymmetric stretching strongly coupled with the $\text{C}^6-\text{H}/\text{N}^7-\text{H}$ in-plane rocking, which are Raman active and provide a rationale for the bands around 1600 cm^{-1} and 1640 cm^{-1} . Furthermore, a large redshift of the backbone carbonyl stretching frequency is predicted for the intermediate from clavulanic acid. Indeed, because of the polarization induced by the environmental electrostatic field, the $\text{C}=\text{O}$ frequency may nearly overlap with the amide I band and the asymmetric stretching mode delocalized on the trans-enamine moiety. Based on these findings, it is proposed that the $\text{C}=\text{O}$ stretch gives rise to a well resolved peak in the experimental spectrum of *d*-clavulanate intermediate.

It has been found that anharmonicity plays a major role in determining both frequencies and intensities, and it is the main reason for the discrepancies between INMA and QM/MM spectra. The importance of anharmonic effects in Raman (and also in infrared) spectra have been recently evidenced for alanine and proline zwitterions in solution (modeled as

a polarizable continuum).⁴⁷ The effects observed in the present study are however more pronounced than those reported for these amino acids. In addition, the comparison between the present QM/MM and INMA spectra calculated with and without the environment embedding potential clearly shows that the surrounding dynamically modulates the Raman activity, enhancing or inhibiting it. For instance, a vibrational mode due to the CH₂ twistings in the intermediate from clavulanic acid is Raman active only in the spectrum calculated from the ACF and only when the modulation by the environment field is accounted.

A major source of error in the calculation of the spectrum from QM/MM simulations comes from the limited phase space sampling, which implies (large) inaccuracies in the ACF. Nevertheless, hybrid QM/MM simulations combined with efficient protocols for the calculation of the polarizability of the target substrate seems to be a fast way to obtain a reasonably accurate description of the vibrational Raman effect. For example, the calculation of the Raman spectrum of the intermediate from clavulanic acid, from the preliminary classical force field simulations to the calculation of polarizability, took about 45 days on 16 cores of an AMD Opteron dual-processor dual-core cluster. In conclusion, our study demonstrates that a reliable and (computationally) efficient calculation of vibrational spectra of large biomolecular complexes can be (almost) routinely employed to help assign the experimental collected data. Probably more important, computational vibrational spectroscopy might become a precious tool for refinement of theoretical models when no other structural information is available.

We conclude remarking that, although the trans-enamine species is the most abundant reaction intermediate and the present study succeeds in interpreting most of the recorded spectral features, further calculations on other possible intermediates (imine and cis-enamine) are required for a more exhaustive understanding of the experimental spectra⁵ and, therefore, the inhibition mechanism.

Acknowledgment. The authors acknowledge computational support from INFM and CINECA. M.S.H. would like to acknowledge the Department of Veterans Affairs in Cleveland for the support of a Career Development Award.

Supporting Information Available: Estimate of the uncertainty in both position and intensity of bands in the calculated Raman spectrum for the clavulanate intermediate. This material is available free of charge via the Internet at <http://pubs.acs.org>.

References

- (1) Helfand, M. S.; Totir, M. A.; Carey, M. P.; A, M, H.; Bonomo, R. A.; Carey, P. R. *Biochemistry* **2003**, *42*, 13386–13392.
- (2) Helfand, M. S.; Taracila, M. A.; Totir, M. A.; Bonomo, R. A.; Buynak, J. D.; van den Akker, F.; Carey, P. R. *Biochemistry* **2007**, *46*, 8689–8699.
- (3) Carey, P. R. *Annu. Rev. Phys. Chem.* **2006**, *57*, 527–554.
- (4) Padayatti, P. S.; Helfand, M. S.; Totir, M. A.; Carey, M. P.; Carey, P. R.; Bonomo, R. A.; van den Akker, F. *Biochemistry* **2004**, *43*, 843–848.
- (5) Kalp, M.; Totir, M. A.; Buynak, J. D.; Carey, P. R. *J. Am. Chem. Soc.* **2009**, *131*, 2338–2347.
- (6) Bonomo, R. A.; Rice, L. B. *J. Gerontol A-Biol* **1999**, *4*, B260–B267.
- (7) Miani, A.; Raugei, S.; Carloni, P.; Helfand, M. *J. Phys. Chem. B* **2007**, *111*, 2621–2630.
- (8) Klähn, M.; Mathias, G.; Kötting, C.; Nonella, M.; Schlitter, J.; Gerwert, K.; Tavan, P. *J. Phys. Chem. A* **2004**, *108*, 6186–6194.
- (9) Nonella, M.; Mathias, G.; Tavan, P. *J. Phys. Chem. A* **2003**, *107*, 8638–8647.
- (10) Cui, Q.; Karplus, M. *J. Chem. Phys.* **2000**, *112*, 1133–1149.
- (11) Case, D.; III, T. C.; Darden, T.; Gohlke, H.; Luo, R.; Jr, K. M.; Onufriev, A.; Simmerling, C.; Wang, B.; Woods, R. *J. Comput. Chem.* **2005**, *26*, 1668–1688.
- (12) Jorgensen, W. L.; Chandrasekhar, J.; Madura, J. D.; Impey, R. W.; Klein, M. L. *J. Chem. Phys.* **1983**, *70*, 926–935.
- (13) Wang, J.; Wolf, R. M.; Caldwell, J. W.; Kollman, P. A.; Case, D. A. *J. Comput. Chem.* **2004**, *25*, 1157–1174.
- (14) Becke, A. D. *J. Chem. Phys.* **1993**, *98*, 5648–5652.
- (15) Wang, J.; Wang, W.; Kollman, P. A.; Case, D. A. *J. Mol. Graphics Modell.* **2006**, *25*, 247–260.
- (16) Frisch, M. J.; Trucks, G. W.; Schlegel, H. B.; Scuseria, G. E.; Robb, M. A.; Cheeseman, J. R.; Montgomery, J. A., Jr.; Vreven, T.; Kudin, K. N.; Burant, J. C.; Millam, J. M.; Iyengar, S. S.; Tomasi, J.; Barone, V.; Mennucci, B.; Cossi, M.; Scalmani, G.; Rega, N.; Petersson, G. A.; Nakatsuji, H.; Hada, M.; Ehara, M.; Toyota, K.; Fukuda, R.; Hasegawa, J.; Ishida, M.; Nakajima, T.; Honda, Y.; Kitao, O.; Nakai, H.; Klene, M.; Li, X.; Knox, J. E.; Hratchian, H. P.; Cross, J. B.; Bakken, V.; Adamo, C.; Jaramillo, J.; Gomperts, R.; Stratmann, R. E.; Yazyev, O.; Austin, A. J.; Cammi, R.; Pomelli, C.; Ochterski, J. W.; Ayala, P. Y.; Morokuma, K.; Voth, G. A.; Salvador, P.; Dannenberg, J. J.; Zakrzewski, V. G.; Dapprich, S.; Daniels, A. D.; Strain, M. C.; Farkas, O.; Malick, D. K.; Rabuck, A. D.; Raghavachari, K.; Foresman, J. B.; Ortiz, J. V.; Cui, Q.; Baboul, A. G.; Clifford, S.; Cioslowski, J.; Stefanov, B. B.; Liu, G.; Liashenko, A.; Piskorz, P.; Komaromi, I.; Martin, R. L.; Fox, D. J.; Keith, T.; Al-Laham, M. A.; Peng, C. Y.; Nanayakkara, A.; Challacombe, M.; Gill, P. M. W.; Johnson, B.; Chen, W.; Wong, M. W.; Gonzalez, C.; Pople, J. A. *Gaussian 03, Revision C.02*.
- (17) Berendsen, H. J. C.; Postma, J. P. M.; DiNola, A.; Haak, J. R. *J. Chem. Phys.* **1984**, *81*, 3684–3690.
- (18) van der Spoel, D.; Lindahl, E.; Hess, B.; Groenhof, G.; Mark, A. E.; Berendsen, H. J. C. *J. Comput. Chem.* **2005**, *26*, 1701–1718.
- (19) Car, R.; Parrinello, M. *Phys. Rev. Lett.* **1985**, *55*, 2471–2474.
- (20) Marx, D.; Hutter, J. Ab initio molecular dynamics: Theory and Implementation. In *Modern Methods and algorithms of quantum chemistry*; Grotendorst, J., Ed.; John von Neumann Institute for Computing: Jülich, 2000; NIC series, Vol. 1, pp 301–349.
- (21) Laio, A.; VandeVondele, J.; Rothlisberger, U. *J. Chem. Phys.* **2002**, *116*, 6941–6947.
- (22) Laio, A.; VandeVondele, J.; Rothlisberger, U. *J. Phys. Chem. B* **2002**, *106*, 7300–7307.
- (23) Becke, A. D. *Phys. Rev. A* **1988**, *38*, 3098–3100.

- (24) Lee, C.; Yang, W.; Parr, R. G. *Phys. Rev. B* **1988**, *37*, 785–789.
- (25) Troullier, N.; Martins, J. L. *Phys. Rev. B* **1991**, *43*, 1993–2006.
- (26) See, e. g.; Sprik, M.; Hutter, J.; Parrinello, M. *J. Chem. Phys.* **1996**, *105*, 1142. Giannozzi, P. In *Computational Approaches to Novel Condensed Matter Systems, Proceedings of 3rd Gordon Godfrey Workshop on Condensed Physics*; Neilson, D., Das, M. P., Ed.; Plenum: New York, 1995.
- (27) Hutter, J.; Alavi, A.; Deutch, T.; Bernasconi, M.; Goedecker, S.; Marx, D.; Tuckerman, M.; Parrinello, M. CPMD; Copyright IBM Corp 1990–2008, Copyright MPI fur Festkorperforschung Stuttgart 1997–2001. <http://www.cpmd.org/> (accessed month day, year).
- (28) Wang, J.; Cieplak, P.; Kollman, P. A. *J. Comput. Chem.* **2000**, *21*, 1049–1074.
- (29) Marthyna, G. J.; Klein, M. L.; Tukerman, M. E. *J. Chem. Phys.* **1992**, *97*, 2635.
- (30) T, H.; Dunning, J. *J. Chem. Phys.* **1989**, *90*, 1007–1023.
- (31) Hall, G. G.; Smith, C. M. *Int. J. Quantum Chem.* **1984**, *25*, 881–890.
- (32) Smith, C. M.; Hall, G. G. *Theor. Chim. Acta* **1986**, *69*, 63–69.
- (33) Hay, P. J.; Wadt, W. R. *J. Chem. Phys.* **1985**, *82*, 270–283.
- (34) Gordon, R. G. *J. Chem. Phys.* **1965**, *42*, 3658–3664.
- (35) McQuarrie, D. A. *Statistical Mechanics*; Harper Collins Publisher: New York, 1973.
- (36) Bader, J. S.; Berne, B. J. *J. Chem. Phys.* **1994**, *100*, 8359–8366.
- (37) Herzberg, G. *Molecular Spectra and Molecular Structure*; Krieger Publishing Company: 1991, Vol. 2.
- (38) Porezag, D.; Pederson, M. *Phys. Rev. B* **1996**, *54*, 7830–7836.
- (39) Chaban, G. M.; Gerber, R. B. *Theor. Chem. Acc.* **2008**, *120*, 273–279.
- (40) Martinez, M.; Gaigeot, M. P.; Borgis, D.; Vuilleumier, R. *J. Chem. Phys.* **2005**, *125*, 144106.
- (41) Wheeler, R. A.; Dong, H. *ChemPhysChem* **2003**, *4*, 1227–1230.
- (42) Max, J.-J.; Chapados, C. *J. Chem. Phys.* **2004**, *120*, 6625–6641.
- (43) Zhang, X. K.; Lewars, E. G.; March, R. E.; Parnis, J. M. *J. Phys. Chem.* **1993**, *97*, 4320–4325.
- (44) Dong, J.; Lu, X.; Wei, Y.; Luo, L.; Dunaway-Mariano, D.; Carey, P. R. *Biochemistry* **2003**, *42*, 9482–9490.
- (45) Marzari, N.; Vanderbilt, D. *Phys. Rev. B* **1997**, *56*, 12847–12862.
- (46) Carnevale, V.; Raugei, S.; Micheletti, C.; Carloni, P. *J. Chem. Phys. B* **2007**, *111*, 12327–12332.
- (47) Daněček, P.; Kapitán, J.; Baumruk, V.; Bednárová, L.; Jr., V. K.; Bouř, P. *J. Chem. Phys.* **2007**, *126*, 224513.

CT900131Q